Scaling of the Bicoid morphogen gradient by a volume-dependent production rate

David Cheung[1], Cecelia Miles[2], Martin Kreitman[2] and Jun Ma[1,3,*]

SUMMARY

An important feature of development is the formation of patterns that are proportional to the overall size of the embryo. But how such proportionality, or scaling, is achieved mechanistically remains poorly understood. Furthermore, it is currently unclear whether organisms utilize similar or distinct mechanisms to achieve scaling within a species and between species. Here we investigate within-species scaling mechanisms for anterior-posterior (A-P) patterning in *Drosophila melanogaster*, focusing specifically on the properties of the Bicoid (Bcd) morphogen gradient. Using embryos from lines artificially selected for large and small egg volume, we show that large embryos have higher nuclear Bcd concentrations in the anterior than small embryos. This anterior difference leads to scaling properties of the Bcd gradient profiles: in broad regions of the large and small embryos along the A-P axis, normalizing their positions to embryo length reduces the differences in both the nuclear Bcd concentrations and Bcd-encoded positional information. We further trace the origin of Bcd gradient scaling by showing directly that large embryos have more maternally deposited *bcd* mRNA than small embryos. Our results suggest a simple model for how within-species Bcd gradient scaling can be achieved. In this model, the Bcd production rate, which is dependent on the total number of *bcd* mRNA molecules in the anterior, is scaled with embryo volume.

KEY WORDS: Bicoid, *Drosophila*, Embryo size, Evolution, Morphogen gradient, Scaling

INTRODUCTION

One of the most intriguing aspects of embryonic development is the proportionality in pattern formation. Despite size variation among individuals in a population their body parts are formed in a proportionate, or scaled, manner (Flatt, 2005; Hendrikse et al., 2007; Patel and Lall, 2002; Waddington, 1942). Scaled patterning is generally robust to genetic background variation and environmental fluctuations, and it takes place within a species as well as across different species. Thus, understanding the mechanistic underpinnings of scaled patterning is important to both evolutionary and developmental biology. Since positional information in pattern formation is initiated by the establishment of concentration gradients of morphogens (Kerszberg and Wolpert, 2007; Lander, 2007; Martinez Arias and Hayward, 2006), a critical component of scaling may occur in the context of the molecular properties of morphogen gradients.

Drosophila Bicoid (Bcd) is one of the best-studied morphogen systems (Driever and Nüsslein-Volhard, 1988a; Ephrussi and St. Johnston, 2004). It forms a concentration gradient along the anterior-posterior (A-P) axis and instructs patterning by activating its downstream targets in a concentration-dependent manner (Burz et al., 1998; Driever and Nüsslein-Volhard, 1988b; Ma et al., 1996; Struhl et al., 1989). Although scaling of patterning along the A-P axis is a well-documented phenomenon (Houchmandzadeh et al., 2002; Lott et al., 2007), there are relatively few mechanistic studies

on the scaling properties of the Bcd gradient. This is in part due to technical difficulties. Unlike the downstream target genes that have sharp boundaries to their expression patterns, the smooth Bcd gradient profile poses significant technical challenges in quantitatively evaluating its properties (Gregor et al., 2007a; He et al., 2008; Reinitz, 2007). In addition, embryos from standard *Drosophila* lines have relatively small variations in size (Gregor et al., 2007a; He et al., 2008; Houchmandzadeh et al., 2002; Lott et al., 2007), further hindering quantitative investigations of scaling mechanisms of the Bcd gradient. Thus, despite its fundamental nature, how Bcd gradient and A-P patterning scaling is achieved mechanistically remains poorly understood and controversial (de Lachapelle and Bergmann, 2010b; Gregor et al., 2005; He et al., 2008; Houchmandzadeh et al., 2002; Manu et al., 2009).

The Bcd profile can be approximated by an exponential function of distance x, $B=Ae^{-x/\lambda}$, where A is the amplitude and λ is the length constant (Houchmandzadeh et al., 2002). Gregor et al. took advantage of embryos from different dipteran species that differ greatly in size and found that λ differed between the species and was correlated with a nearly fivefold difference in the embryo length, L (Gregor et al., 2005). According to a simple diffusion model (Wartlick et al., 2009; Wolpert, 1969), λ is a function of the diffusion constant D and the decay rate ω of the morphogen molecules: $\lambda^2=D/\omega$. Within the framework of this model, between-species scaling for the Bcd gradient is likely to be achieved through species-specific evolution of the diffusion and/or decay rates (Gregor et al., 2005; Gregor et al., 2008).

Whether and how the Bcd gradient profiles are scaled within a species remains controversial and less well understood. It has been suggested that, unlike the scaling properties observed in embryos across different species, the Bcd gradient within a species is not scaled with L (Gregor et al., 2005). However, our own studies have shown that Bcd gradient profiles in wild-type (wt) *D. melanogaster* embryos exhibit properties indicative of scaling (He et al., 2008).

[1]Division of Biomedical Informatics, Cincinnati Children's Research Foundation, 3333 Burnet Avenue, Cincinnati, OH 45229, USA. [2]Department of Ecology and Evolution, The University of Chicago, 1101 E 57 Street, Chicago, IL 60637, USA. [3]Division of Developmental Biology, Cincinnati Children's Research Foundation, 3333 Burnet Avenue, Cincinnati, OH 45229, USA.

*Author for correspondence (jun.ma@cchmc.org)

The role of Bcd-encoded positional information in within-species scaling is a matter of current debate (de Lachapelle and Bergmann, 2010a; de Lachapelle and Bergmann, 2010b; Jaeger, 2010).

Whereas stochastic fluctuations in egg size in a genetically inbred population only lead to modest size differences, genetic variation for egg size in natural populations does exist. In a forced selection experiment based on a collection of 120 females from central Illinois, Miles et al. produced population cages of *D. melanogaster* exhibiting, on average, a 37.9% difference in egg volume between the large and small egg selected cages (Miles et al., 2010). Despite the significant size differences between the embryos from these selected populations, the expression boundary positions for the pair-rule gene *even skipped* (*eve*) exhibit good scaling properties (Miles et al., 2010). We reasoned that the Bcd gradient properties in these embryos, and in a pair of inbred lines derived from them, might provide insights into how scaled A-P patterning is achieved within a species. In particular, do Bcd gradient profiles in embryos that are genetically divergent for egg size exhibit scaling properties? If so, does the length constant λ of the Bcd gradient differ between the lines as a means for achieving scaling (as it apparently does between species)?

Our results show that, in broad regions of the large and small embryos, normalizing their A-P positions to L reduces the differences in both the Bcd concentrations and its encoded positional information, properties indicative of scaling. We further show that, unlike between-species scaling, the Bcd gradient profiles have similar λ but differ in Bcd concentrations at the anterior, B_0, that are scaled with embryo volume. We directly trace the origin of within-species Bcd gradient scaling by measuring the amount of the maternally deposited *bcd* mRNA in early embryos. We show, for the first time to our knowledge, that large embryos have more *bcd* mRNA than small embryos. Our results suggest that scaling of the Bcd production rate with embryo volume represents one mechanism by which Bcd gradient scaling can be achieved. Taken together, our study significantly advances understanding of the origin of within-species scaling for the Bcd morphogen gradient. It also reveals how organisms may achieve within-species and between-species Bcd gradient scaling through distinct, although not necessarily mutually exclusive, mechanisms.

MATERIALS AND METHODS
Fly strains, artificial selection and inbreeding
Replicate populations of *D. melanogaster* with divergent egg sizes were generated using artificial selection from a collection of 120 wild-caught females from central Illinois, USA (Miles et al., 2010). Briefly, truncation selection from January 2007 through June 2008 resulted in three replicate cages each of large egg-producing and small egg-producing populations. Mean egg volume of the base population ($\pm$ s.e.) was $10.3\pm0.03\times10^{-3}$ mm^3. Mean egg volumes among lines for the large and small egg cages after selection were $12.1\pm0.02\times10^{-3}$ mm^3 and $8.7\pm0.02\times10^{-3}$ mm^3, respectively, representing a difference in egg length of ~12%. As shown previously (Miles et al., 2010), embryos from these lines, despite their size difference, exhibit good scaling properties along the A-P axis as measured by the *eve* expression boundary positions.

After cessation of selection, populations were allowed to randomly mate within the six replicate cages and environmental conditions were held constant. Cages #2 and #9, with large and small embryos, respectively, were used in our current work. Embryos used in this study were collected 9 months after selection was stopped (March 2009). Each cage represented a randomly mating population of flies that, despite having undergone directional selection on egg size, still possessed considerable genetic variation segregating in each generation. Embryo length in the cages had regressed toward the mean slightly (see Fig. S1 legend in the supplementary material for measurements). To obtain pure-breeding

genetically stable lines differing in egg size, we established inbred lines as follows. Virgin females from each cage were mated with individual brothers to initialize each inbred line. Brother-sister inbreeding continued from July 2008 through June 2010. In every generation females were mated with brothers but virgins were not routinely collected. A pair of inbred lines (#2.46 and #9.17) derived from the original cages #2 and #9, respectively, was used in our current analysis. Embryos used in our work were collected after 30 generations of full-sib inbreeding (January 2010). To make a distinction with the embryos from the population cages (with their Bcd data shown in Figs S1-S4 in the supplementary material), we refer to these embryos as the inbred or purebred embryos (with their Bcd data shown in Figs 1-3).

For our current work, 0-1 hour embryo collections were used for *bcd* mRNA fluorescence in situ hybridization (FISH) experiments and 0-4 hour collections for Bcd immunostaining experiments. All embryos were collected at 25°C. Fly lines for calibrating *bcd* mRNA measurements were as follows: *Df(3R)BSC467/TM6C Sb^1 cu^1* (for 1×*bcd*; Bloomington stock 24971), *w^{1118}* (for 2×*bcd*) and *Sp/CyO-bcd$^+$*; *Dr/TM6B* (for 3×*bcd*; the *CyO-bcd$^+$* chromosome was from a line kindly provided by Dr Gary Struhl (Struhl et al., 1989).

Immunostaining and data analysis
For antibody staining, embryos were collected and fixed as previously described (Kosman et al., 1998), with an additional post-fixation step and permeabilization treatment (He et al., 2008; Patel et al., 2001). The primary and secondary antibodies were, respectively, a polyclonal rabbit anti-Bcd (Santa Cruz Biotechnology) and Alexa Fluor 594 goat anti-rabbit (Molecular Probes). Nuclei were counterstained using 4′,6-diamidino-2-phenylindole dihydrochloride (DAPI, Sigma). Stained embryos were mounted in DABCO anti-fade mounting media (Sigma) onto slides with bridges. High-resolution digital images (1388×1040, 8 bits/pixel) were captured on a Zeiss Imager Z1 ApoTome microscope with a Zeiss Plan 10× Aprochromat objective using Axiovision 4.5 software in the linear setting without any normalization or adjustments. Embryos were oriented laterally for imaging the midsagittal section.

Fluorescence intensities were extracted from the nuclear layer on the dorsal side of embryos at early nuclear cycle 14 as described previously (He et al., 2008). For background measurement, we added embryos from *bcd^{E1}* females to each group of experimental embryos; background subtraction was performed for individual groups separately. All parameter calculations were performed using Matlab (R2008b version 7.7) including the Statistics Toolbox (MathWorks). The length constant values were calculated for individual embryos by a linear fitting of $\ln(B/B_{max})$ against x or x/L, where both B and B_{max} are background-subtracted without other adjustments as described previously (He et al., 2008; Liu and Ma, 2011). The intensity values within the range $x/L=0.1$ to 0.5 were used in all calculations of length constant values. The Bcd intensity data presented in this work are available upon request.

FISH and data analysis
All embryos used in FISH were collected, fixed and permeabilized as described above. Digoxigenin-11-UTP (Roche Applied Science) labeled RNA probe was generated from a *bcd* cDNA plasmid [FY441 (Zhao et al., 2002)] and hybridized with the embryos for 72 hours at 60°C. The primary antibody was mouse anti-digoxigenin (Roche Applied Science); the secondary antibody was goat anti-mouse Alexa Fluor 555 (Molecular Probes). Nuclear counterstaining, embryo mounting and imaging were as described above except without engaging ApoTome mode.

For image processing, we first used the DAPI counterstain background signals to demarcate the outline of the embryo. We then used Otsu's method (Otsu, 1979) to determine the threshold for specific signals and generated a contour line, the area within which was used for signal extraction. Background was subtracted using the mirror image of the measuring area positioned at the posterior end of the embryo using Matlab. Owing to the morphological differences between the anterior and posterior tips of the embryos, it was necessary to make minor adjustments to properly position the background measuring area, which was first placed at the posterior tip of the embryo and then scanned for the first location at

which it was fully contained within the bounds of the embryo outline. The method of using an inversed area for background subtraction provides a way to correct for uneven distributions of background signals in whole-mount embryos (Myasnikova et al., 2005) and for embryo-to-embryo variations in both *bcd* mRNA distributions and background signals.

Calculation of embryo volume assumes a prolate spheroid shape ($V = \pi L H^2/6$, where L is embryo length and H is embryo height). All embryos in this study (for both protein staining and mRNA FISH) were imaged on slides under bridged coverslips to minimize geometric distortion. When describing the relative difference between the average lengths (or volumes) of the embryos, we also provide an error estimate, which was calculated as the s.d. of the relative differences between individual large and small embryos in all possible pairs. All *P*-values are from Student's *t*-tests unless stated otherwise.

RESULTS

Large and small embryos have different nuclear Bcd concentrations in the anterior

To investigate mechanisms of scaled A-P patterning in *Drosophila*, we took advantage of the large and small embryos produced by artificially selected lines (Miles et al., 2010). In our current work, embryo size refers to the volume of the embryo; these two terms are used interchangeably and they are distinct from the length of the embryo. As detailed in the Materials and methods, we analyze embryos from both the originally selected population cages (#2 and #9) and from a pair of inbred lines derived from these cages (#2.46 and #9.17). Cages #2 and #9, and their corresponding inbred lines #2.46 and #9.17, have large and small embryos, respectively. We performed quantitative fluorescence immunostaining to detect Bcd in both sets of embryos. For conciseness, our Bcd staining results from the embryos from the inbred lines are presented as main figures, whereas the corresponding results from embryos from the population cages are shown in supplementary figures. Although the difference in size between embryos from the two population cages is smaller than between embryos from the two inbred lines (as expected, see Materials and methods), the two sets of data are consistent with each other (see Fig. S1 in the supplementary material for further details).

To ensure a direct comparison between our detected Bcd intensities in stained embryos, the large and small embryos were stained side by side, with images captured within a linear range in a single imaging cycle under identical settings, including the exposure time. To facilitate background measurements under identical staining conditions, we also mixed embryos from *bcd*[E1] females with our experimental embryos. Fig. 1A,C shows midsagittal fluorescence images of representative large and small embryos at early nuclear cycle 14. To help visualize the shape and size of these embryos, images showing nuclei are displayed next to their corresponding fluorescence images (Fig. 1B,D). A visual inspection of these images gives an immediate, non-quantitative impression: the raw fluorescence intensities for Bcd are higher in the large embryo than in the small embryo.

To quantify our immunostaining data, we extracted the Bcd intensity values within the nuclear layer of the midsagittal images. As discussed previously (He et al., 2008), these extracted Bcd intensity values have a linear relationship with nuclear Bcd concentrations. Fig. 1E-H shows the raw Bcd intensity, *B*, in the large and small embryos as a function of either the absolute distance from the anterior (*x*, in μm) or of relative distance (*x/L*; see Fig. S1A-D in the supplementary material for corresponding data for embryos from population cages). In these figures, the measured background intensities are also shown. Our quantitative results (*n*=9 for both groups) confirm the visual impression and
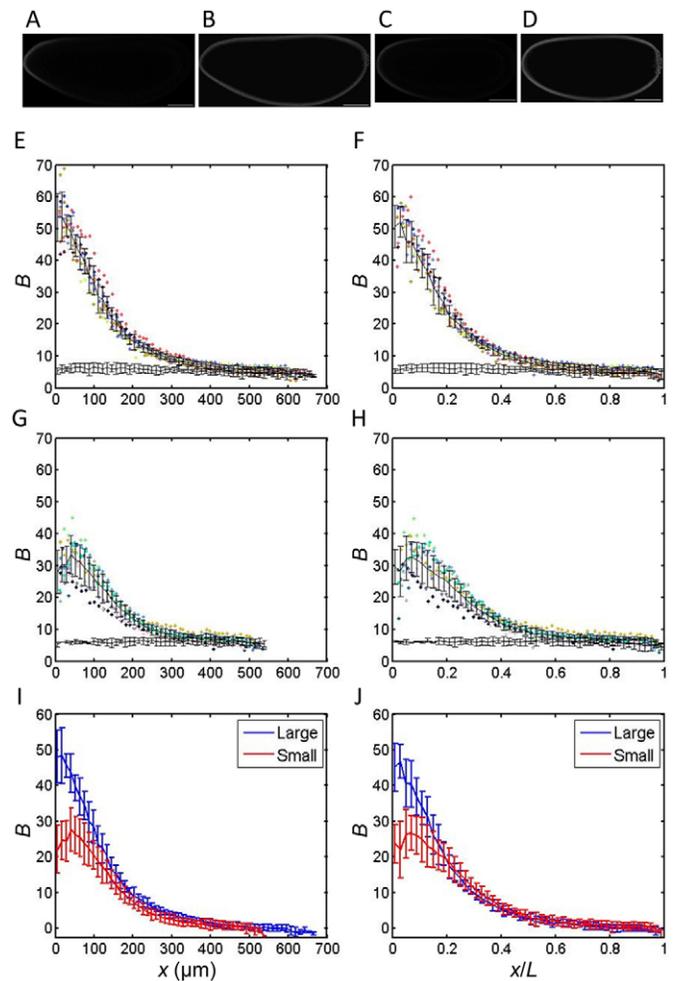

Fig. 1. Quantitative measurements of Bcd intensities from large and small *Drosophila* embryos. (**A-D**) Raw midsagittal fluorescence images of representative large (A) and small (C) embryos immunostained for Bcd, and their corresponding DAPI images (B,D). Large and small embryos are from inbred lines #2.46 and #9.17, respectively. A and C were captured within linear range without any adjustments. For presentation purposes, B and D have had their fluorescence intensities adjusted. (**E-H**) The Bcd fluorescence intensity, *B*, from purebred large (E,F) and small (G,H) embryos expressed as a function of *x* (E,G) or *x/L* (F,H); *n*=9 for both groups. Mean ± s.d. of *B* is shown at each position. Each color represents data from an individual embryo. Also shown are the background intensities (mean ± s.d.) extracted from images of embryos from *bcd*[E1] females (F shows background intensities only from the relevant regions of the embryos). (**I,J**) The mean Bcd intensity profiles from purebred large and small embryos as a function of *x* (I) or *x/L* (J). All *B* values presented are background-subtracted without any further adjustments, with the exception of E-H and Fig. S1A-D in the supplementary material, where raw intensity values are presented without background subtraction. Error bars indicate s.d.

demonstrate that the raw Bcd intensities in large embryos are higher than in small embryos. In particular, the nuclear Bcd concentrations (in arbitrary intensity units) at the anterior, B_0, are 45.1±6.7 and 23.7±5.4 (mean ± s.d.) for the large and small embryos, respectively ($P=1.2\times10^{-6}$; Student's *t*-test). Throughout this work (except the raw intensity data shown in Fig. 1E-H and Fig. S1A-D in the supplementary material), all Bcd intensity values

have been background-subtracted without any further adjustments. The maximal nuclear Bcd concentration, B_{max}, is also significantly higher in large embryos than in small embryos (49.4±3.3 versus 29.6±4.8, respectively; $P=2.2\times10^{-8}$; see Fig. S2 in the supplementary material for measurements of B_0 and B_{max} from individual embryos). These results are consistent with our previous findings obtained from a population of wt embryos that exhibited small variations in embryo size (He et al., 2008), but the enhanced embryo size difference found in our current study resulted in greater differences in both B_0 and B_{max} (see Fig. S1 legend in the supplementary material for further evidence supporting this conclusion). Together, our results demonstrate that the nuclear Bcd concentrations in the anterior are higher in large embryos than in small embryos.

Bcd gradient profiles from large and small embryos converge as a function of *x/L*

To directly compare the measured Bcd gradient profiles in the large and small embryos, we plot in same graphs their mean profiles as a function of either *x* (Fig. 1I) or *x/L* (Fig. 1J). Our results show that, although the two profiles are visibly different from each other when expressed as a function of *x*, they exhibit a property of convergence, as a function of *x/L*, in broad regions of the embryo along the A-P axis, except at their most anterior parts (see Fig. S1E,F in the supplementary material for corresponding data for embryos from population cages). Such convergence – a reduction in the difference between these two Bcd gradient profiles in broad regions of the embryo (except their most anterior regions) when using A-P positions relative to embryo length – is a hallmark of scaling (Deng et al., 2010; He et al., 2008).

To further evaluate this convergence, or scaling, of the Bcd gradient profiles, we performed three additional analyses. First, we calculated the difference between the mean nuclear Bcd concentrations in large and small embryos, ΔB, at different A-P positions. Fig. 2A,B shows ΔB, normalized to the averaged concentrations from the large and small embryos, $\langle B\rangle$, as a function of *x* or *x/L* (see Fig. S3A,B in the supplementary material for corresponding data for embryos from population cages). For this analysis, we focused on the anterior half of the embryo where the measured Bcd intensities are more reliable due to lower experimental and background errors (He et al., 2010a; He et al., 2010b; He et al., 2008). The plots in Fig. 2A and 2B show data from equivalent regions of the embryo so as to allow direct comparison, i.e. the display windows for *x* when normalized to $\langle L\rangle$ (Fig. 2A) and *x/L* (Fig. 2B) are equivalent. Although $\Delta B/\langle B\rangle$ in the anterior is, as expected, similar between these two plots, it quickly diverges as we move away from the anterior. In particular, whereas $\Delta B/\langle B\rangle$ as a function of *x* remains relatively stable and stays as a positive value throughout the entire A-P length in the display (Fig. 2A), it exhibits a significant drop as a function of *x/L* to settle near zero (Fig. 2B). This illustrates that, in broad regions of the large and small embryos along the A-P axis (except in their most anterior regions), normalization of their A-P positions to *L* reduces the differences in their nuclear Bcd concentrations.

In a second analysis, we calculated the difference between large and small embryos in the positions at which the mean Bcd gradient profiles cross different Bcd concentration thresholds. We plot this difference in terms of positional information, Δx, as a function of either *x* or *x/L* (Fig. 2C,D and see Fig. S3C,D in the supplementary material for corresponding data for embryos from population cages). To facilitate a comparison between these two plots, we use $\Delta x/\langle L\rangle$ in Fig. 2C, where $\langle L\rangle$ is the averaged length of the large and
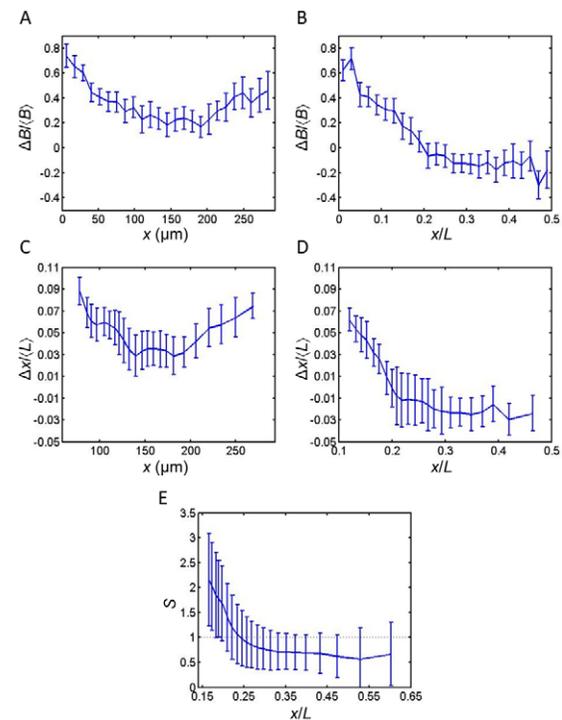

Fig. 2. Quantitative analyses demonstrating Bcd gradient scaling. (**A**,**B**) Differences between the mean Bcd fluorescence intensities from the purebred large and small *Drosophila* embryos, ΔB, as a function of *x* (A) or *x/L* (B). Here, ΔB is normalized to the averaged Bcd intensities from large and small embryos, $\langle B\rangle$. Error bars indicate s.d. of the difference between the sample means, estimated as $\sqrt{(\sigma_1^2/n_1)+(\sigma_2^2/n_2)}$, where σ_1 and σ_2 are Bcd intensity s.d. from the large and small embryos, respectively, and n_1 and n_2 are their respective sample sizes. (**C**,**D**) Differences in Bcd-encoded positional information between the purebred large and small embryos expressed as a function of *x* (C) or *x/L* (D). Here, Δx and $\Delta x/L$ denote the differences between the A-P positions at which the mean Bcd profiles from the large and small embryos cross given Bcd thresholds. We used interpolated *B* values to find the A-P positions (*x* or *x/L*) at different thresholds. To facilitate a direct comparison between C and D, Δx in C is normalized to the mean length of the large and small embryos, $\langle L\rangle$. Error bars represent s.d. of the difference between the sample mean positions, estimated (see above) from the positional errors for the large and small embryos converted from their respective intensity errors as described previously (Gregor et al., 2007a). See text for further details. (**E**) Scaling coefficient *S* as a function of A-P position. This analysis was conducted by pooling the data from the large and small embryos, which have a mean length of $\langle L\rangle$. The position x_i at which the *i*th Bcd profile crosses a threshold was obtained from its interpolated *B* values (after the use of Matlab's Smooth function). The mean of the positions at which individual profiles cross this threshold is $\langle x\rangle$. Scaling coefficient *S* was calculated as reported (de Lachapelle and Bergmann, 2010b) and is defined as $S=\hat{\beta}\langle L\rangle/\langle x\rangle$, where $\hat{\beta}$ is the estimated slope from a linear regression $x=\alpha+\beta L$ of x_i values onto their respective length L_i values. Error bars indicate 95% confidence intervals from the regression analysis. Technically, and more accurately, *x/L* shown in the figure represents $\langle x\rangle/\langle L\rangle$.

small embryos. As in Fig. 2A,B, Fig. 2C,D show data from equivalent regions of the embryo. Our results show that the difference in the positional information provided by the mean Bcd gradient profiles from the large and small embryos quickly diminishes as a function of *x/L* (Fig. 2D). This property, which stands in contrast to the profile shown in Fig. 2C where Δx persists

as a function of x, is another way of saying that normalizing A-P positions to L reduces the difference between the mean Bcd gradient profiles (in broad regions of these embryos, except their most anterior parts).

Finally, we analyzed the large and small embryos as a pooled group and calculated the scaling coefficient, S, at different positions (de Lachapelle and Bergmann, 2010b). It has been suggested that perfect scaling has an S value of 1, whereas values above and below 1 represent hyperscaling and hyposcaling, respectively. Our results (Fig. 2E) show that, consistent with the expression boundary positions of Bcd target genes (de Lachapelle and Bergmann, 2010b), the S values are significantly higher than 1 in the anterior parts of the embryo, suggestive of hyperscaling. The S value quickly drops toward the middle of the embryo, with the S profile settling close to 1 (see Fig. S3E in the supplementary material for corresponding data for embryos from population cages; see Discussion for further information). Together, these results provide quantitative evidence that the Bcd gradient profiles from the large and small embryos have properties indicative of scaling.

Mechanisms of scaling evaluated by the length constant of Bcd gradient profiles

Previous studies suggest that Bcd gradient scaling across different species is achieved by evolved differences in the balance of diffusion and degradation rates such that λ is scaled with L (Gregor et al., 2005). To determine whether large and small embryos from the selected lines of a single species, *D. melanogaster*, employ a similar mechanism in Bcd gradient scaling, we calculated the length constant values either as an absolute length λ (in µm) or as a relative length λ/L. We found that the Bcd gradient profiles from the large and small embryos have comparable λ values in absolute length [$\lambda=99.2\pm5.7$ µm and 94.0 ± 20.1 µm (mean $\pm$ s.d.), respectively; $P=0.46$, Student's t-test]. By contrast, the relative length constants for these embryos are significantly different from each other ($\lambda/L=0.16\pm0.02$ and 0.19 ± 0.04 for large and small

embryos, respectively; $P=0.015$; see Fig. S4 legend in the supplementary material for length constant values for embryos from population cages).

To further evaluate λ values measured as either absolute length or relative length, we analyzed the mean Bcd gradient profiles from the large and small embryos. Here, we plot $\ln(B/B_{max})$ of the mean profiles as a function of either x (Fig. 3A) or x/L (Fig. 3B). As in the analyses shown in Fig. 2, we exclude data in regions $x/L>0.5$ to minimize the impact of experimental and background errors. We also exclude data from the most anterior parts of the embryo, where the Bcd gradient profiles are known to deviate significantly from the exponential function (He et al., 2010a; He et al., 2008; Houchmandzadeh et al., 2002). To facilitate comparison, the display windows for x when normalized to $\langle L \rangle$ (Fig. 3A) and x/L (Fig. 3B) are equivalent. In the plots shown in Fig. 3A,B, the length constants of the mean Bcd profiles are the negative reciprocals of the slopes. Our results show that, whereas the slopes are similar for the two mean profiles as a function of x, they diverge as a function of x/L, with a steeper slope, and thus a smaller λ/L value, for the mean Bcd gradient profile from the large embryos (see Fig. S4A,B in the supplementary material for corresponding data for embryos from population cages).

Correlation between nuclear Bcd concentration and embryo size

The significant difference between B_0 or B_{max} in large and small embryos (Fig. 1E-J and see Fig. S1A-F in the supplementary material), coupled with the lack of a significant difference in their respective λ values (Fig. 3A), suggest that within-species scaling for the Bcd gradient is established through properties or events that are restricted primarily to the anterior parts of the embryo, as opposed to between-species differences that are manifested throughout the embryo. To evaluate how the differences in the nuclear Bcd concentrations at the anterior of the large and small embryos are propagated as a function of distance, we plot the correlation coefficient between the nuclear Bcd concentration B and embryo length L, r_{B-L}, as a function of either x or x/L (Fig. 3C,D and see Fig. S4C,D in the supplementary material for corresponding data for embryos from population cages). Our results show that, whereas the anterior-initiated r_{B-L} is propagated reliably well into the middle and posterior parts of the embryo as a function of x, it exhibits a precipitous drop in the anterior (at x/L ~0.15) of the embryo. This drop in r_{B-L} directly contributes to the convergence of the mean Bcd gradient profiles from the large and small embryos (see Fig. 1I,J and Fig. S1E,F in the supplementary material).

To better understand the mechanistic basis for Bcd gradient scaling, we asked a simple question: is the observed difference in B_0 or B_{max} between the large and small embryos better explained by their length difference or size (i.e. volume) difference? The large and small embryos from the inbred lines have an average length of 645.7 ± 22.1 µm and 518.6 ± 22.4 µm (mean $\pm$ s.d.), respectively ($P=1.8\times10^{-9}$), representing a 24.5% difference (with an error estimate of 4.2%). Assuming a prolate spheroid embryo shape, the average volume of the large and small embryos is $18.2\pm1.4\times10^3$ mm^{-3} and $10.6\pm1.0\times10^3$ mm^{-3}, respectively ($P=5.3\times10^{-10}$), representing a 71.7% difference (with an error estimate of 6.9%; the height of the large and small embryos is 232.1 ± 6.4 µm and 197.5 ± 7.7 µm, respectively, $P=1.5\times10^{-8}$). We found that the B_{max} difference between the large and small embryos is 66.9% (with an error estimate of 10.1%), which is closer to the embryo volume difference (71.7%) than the embryo length difference (24.5%). The
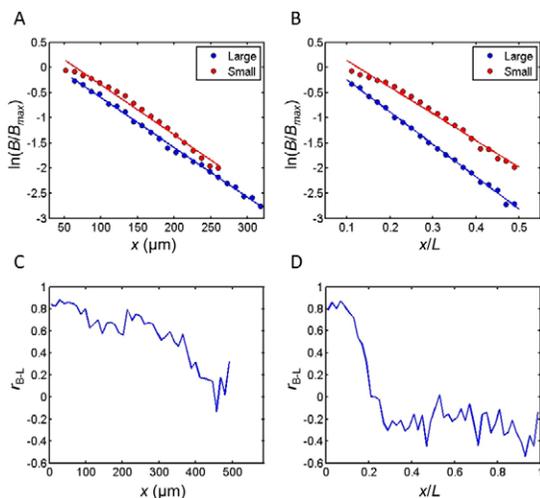

Fig. 3. Length constants and propagation of Bcd intensity differences in large and small embryos. (**A**,**B**) Scatter plots of $\ln(B/B_{max})$ of the mean Bcd fluorescence intensities in the purebred large (blue) and small (red) *Drosophila* embryos against x (A) or x/L (B). Solid lines represent linear fits. (**C**,**D**) Correlation coefficients between B and L, r_{B-L}, as a function of x (C) or x/L (D) for the purebred large and small embryos analyzed together.

difference between the B_0 values from the large and small embryos, 90.3% (with an error estimate of 14.5%), is also closer to the embryo volume difference than the embryo length difference. Our data from embryos collected from the population cages further support this conclusion (for details, see Fig. S2 legend in the supplementary material).

Establishing a method to directly quantify the amount of *bcd* mRNA in embryos

In an idealized simple diffusion model, the steady state concentration of the morphogen molecules at the source, *A*, is a function of the morphogen production rate *J*: $A=J(D\omega)^{-1/2}$, where *D* and ω are, respectively, the diffusion constant and decay rate of the morphogen molecules (He et al., 2010a; Wartlick et al., 2009; Wolpert, 1969). To further trace the origin of Bcd gradient scaling mechanisms, we sought to determine whether the amount of the maternally deposited *bcd* mRNA, and thus the production rate of Bcd protein molecules, might be different between the large and small embryos. But we first needed to develop a method for quantifying *bcd* mRNA in whole-mount embryos. For our study, we used a quantitative fluorescence in situ hybridization (FISH) analysis to detect *bcd* mRNA in embryos. We captured raw epifluorescence intensities within a linear range, without normalization or other adjustments. To minimize the effects of *bcd* mRNA decay (Berleth et al., 1988) or redistribution (Little et al., 2011; Spirov et al., 2009), we specifically selected embryos no later than the fifth nuclear cycle, as judged by the number of nuclei detected by DAPI counterstaining. For calibration, we used embryos from females that have one, two or three copies of *bcd*, referred to as 1×, 2× and 3×*bcd* calibrating embryos, respectively. The 1×*bcd* calibrating embryos were obtained from +/deficiency females, which lacked a copy of the *bcd* gene. Fig. 4A-C shows representative epifluorescence images of 1×, 2× and 3×*bcd* embryos, which were stained side by side, with their images captured under identical settings including the exposure time. A

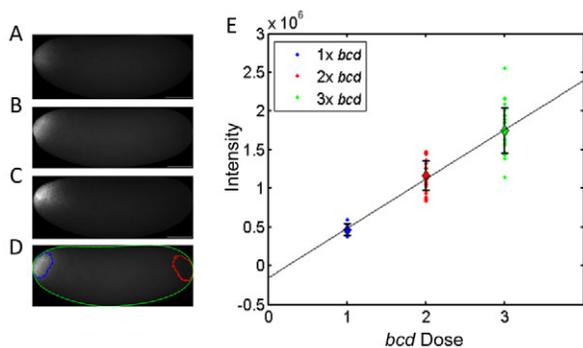visual, non-quantitative inspection reveals that, as expected, epifluorescence signals are lowest in 1×*bcd* embryos and highest in 3×*bcd* embryos.

Since the distributions of *bcd* mRNA exhibit a significant variability among embryos, we developed a method to outline, for individual embryos, the anterior areas from which *bcd* mRNA fluorescence signals were extracted. We used Otsu's thresholding algorithm (Otsu, 1979) to draw a contour line at a threshold established for that embryo. To subtract the non-specific signals present inside the outlined detection areas in the anterior, we inverted the contour shape to the posterior end of the embryo (Fig. 4D; see Materials and methods for details). We used the aggregate epifluorescence intensities extracted from each embryo, with background subtracted individually, to evaluate the relationship between the detected intensities and the relative amounts of *bcd* mRNA in whole-mount embryos. Fig. 4E shows that the intensities detected in the calibrating embryos exhibit a linear relationship with the maternal *bcd* gene dose, demonstrating that our method is adequate for quantitatively measuring the amount of *bcd* mRNA in whole-mount embryos. We used the standard curve shown in Fig. 4E to convert fluorescence intensity to relative *bcd* mRNA amount for experiments that were conducted side by side with these calibrating embryos.
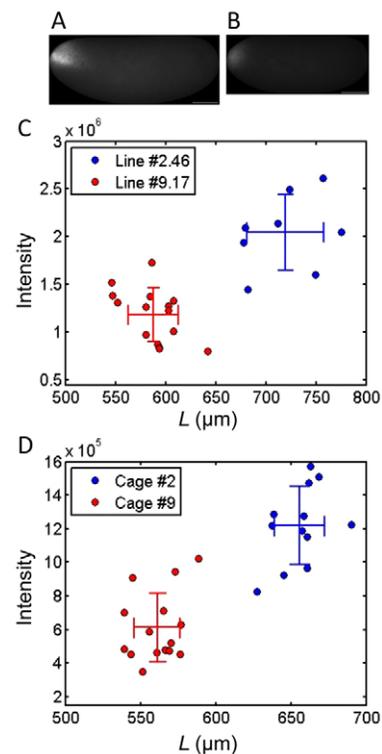

Fig. 4. Establishing procedures for quantitative measurement of *bcd* mRNA. (**A-C**) Epifluorescence images of representative 1× (A), 2× (B) and 3×*bcd* (C) calibrating *Drosophila* embryos. These images were captured within a linear range with an identical exposure time. (**D**) Epifluorescence image of an embryo showing the embryo mask (green), the outlined area for extracting *bcd* mRNA signals (blue) and the posterior area for measuring background signals (red). (**E**) Epifluorescence intensities (in arbitrary units) from 93 embryos plotted against their maternal *bcd* gene dose. Also shown are the mean (± s.d.) for each group of embryos and the linear regression of these values. The linear regression line shown has a function of $y=(6.39x-1.53)\times10^5$, with adjusted $R^2=0.995$.

Fig. 5. Large embryos have more *bcd* mRNA than small embryos. (**A,B**) Epifluorescence images of representative large (A; from cage #2) and small (B; from cage #9) *Drosophila* embryos that have undergone FISH for *bcd*. Both images were captured within a linear range with an identical exposure time and without any adjustments. (**C,D**) Scatter plots of FISH intensities against embryo length. These embryos are from the inbred lines (C) or population cages (D); each pair of embryos was analyzed on a side-by-side basis. Here, the epifluorescence intensity values are in arbitrary units, with background subtracted individually without any further adjustments. Mean ± s.d. is shown.

Large and small embryos have different amounts of maternally deposited *bcd* mRNA

We applied our method described above to the large and small embryos from the selected *D. melanogaster* lines. To minimize experimental errors, each pair of large and small embryos was analyzed on a side-by-side basis (see Fig. 5A,B for representative raw images). Similar to the calibrating embryos, we selected experimental embryos no later than the fifth nuclear cycle in order to minimize the effects of *bcd* mRNA decay or redistribution. Fig. 5C,D shows scatter plots of the measured epifluorescence intensities against L for inbred lines and caged populations, respectively. The large embryos have significantly higher intensities than the small embryos ($P=4.8\times10^{-6}$ and 1.5×10^{-7} for embryos from inbred lines and population cages, respectively; see Figs S5-S7 and Table S1 in the for additional data supportive of this conclusion).

Using the established standard curve (Fig. 4E), we converted the fluorescence intensities to the amount of *bcd* mRNA to assess whether differences in mRNA amount are more consistent with differences in embryo length or embryo volume. We only used data from experiments that were performed side by side with the calibrating embryos shown in Fig. 4E. Here, the large and small embryos (from population cages #2 and #9, respectively) have an average length of 655.8±16.6 μm and 561.3±15.3 μm (mean ± s.d.), respectively ($P=3.0\times10^{-14}$), representing a 16.8% difference (with an error estimate of 3.1%). Their average estimated volume is $20.2\pm1.0\times10^{-3}$ mm^3 and $14.5\pm1.1\times10^{-3}$ mm^3, respectively ($P=8.3\times10^{-13}$), representing a 39.3% difference in volume (with an error estimate of 6.6%; their respective height is 242.3±5.8 and 221.9±7.3 μm, $P=3.1\times10^{-8}$). The relative *bcd* mRNA amount (converted from measured intensities) in these embryos differs by 79.3% (with an error estimate of 18.1%), a value that is closer to the embryo size difference than the embryo length difference (see Fig. S5 legend in the supplementary material for additional results supporting this conclusion). Although our FISH data contain unavoidable errors due to the inherent technical difficulties in accurately quantifying the amount of *bcd* mRNA in whole-mount embryos, they are nonetheless consistent with our Bcd staining data with regard to B_0 and B_{max} in relation to embryo volume (see above). Together, they support the hypothesis that the amount of maternally deposited *bcd* mRNA is set by embryo volume rather than length.

DISCUSSION

Embryonic patterning is a robust process that is insensitive to embryo size (Flatt, 2005; Hendrikse et al., 2007; Houchmandzadeh et al., 2002; Lott et al., 2007; Miles et al., 2010; Patel and Lall, 2002; Waddington, 1942). Our results described here (Fig. 2 and see Fig. S3 in the supplementary material) and in a previous report (He et al., 2008) show that the Bcd gradient profiles in *D. melanogaster* embryos exhibit scaling properties. The enhanced size differences between the embryos from the selected *Drosophila* lines have enabled us to investigate, in greater depth and clarity, Bcd gradient scaling and its origin. We show that large embryos have more maternally deposited *bcd* mRNA than small embryos. The differences between these embryos in both B_0 (or B_{max}) and the amount of *bcd* mRNA are better explained by the differences in embryo volume than embryo length. In an idealized simple diffusion model, the steady state morphogen concentration at the source is a function of the morphogen production rate. If the number of Bcd molecules produced per unit time is proportional to the total number of *bcd* mRNA molecules in the anterior of an embryo, then the aggregate Bcd production rate for the embryo should be proportional to the total amount of maternally deposited *bcd* mRNA. During oogenesis, the majority of *bcd* mRNA is deposited when nurse cells 'dump' their cytoplasmic contents into the oocyte (Weil et al., 2006). If the *bcd* mRNA concentration in these cytoplasmic contents is similar across different egg chambers at the time of dumping, then the total number of *bcd* mRNA molecules in an egg should be approximately proportional to its volume, on average. Based on these considerations and our experimental results, we propose a simple model for how Bcd gradient scaling within a species can be achieved. In this model, deposition of *bcd* mRNA is dependent on egg volume, which leads to a volume-dependent adjustment of the Bcd production rate in the anterior, allowing the Bcd gradient to achieve scaling in broad regions of the embryo. We now discuss several attributes of this model.

Our proposed Bcd gradient scaling model, i.e. a volume-dependent Bcd production rate, represents an early-acting scaling mechanism along the A-P axis in *D. melanogaster* embryos. In addition, since Bcd acts as a direct and sustained input for target gene transcription (He et al., 2010a; He et al., 2010b; He et al., 2008; He et al., 2011; Liu et al., 2011), the scaling properties of the Bcd gradient also represent a critical means by which scaled A-P patterning is achieved in broad regions of the embryo (see below for further discussion).

The proposed volume-dependent production rate mechanism for within-species Bcd gradient scaling differs from the previously identified between-species scaling mechanism (Gregor et al., 2005). Whereas between-species scaling is achieved by evolutionary adjustment of λ to scale it with L (Gregor et al., 2005), our large and small *D. melanogaster* embryos have comparable λ values in absolute length (Fig. 3A,B and see Fig. S4A,B in the supplementary material). In a simple diffusion model (Wartlick et al., 2009; Wolpert, 1969), $\lambda^2=D/\omega$, suggesting that between-species scaling is achieved by adjusting the effective diffusion constant D and/or the effective decay rate ω, species-specific properties that are manifested throughout the embryos (Gregor et al., 2005; Gregor et al., 2008). In our model, Bcd gradient scaling within a species is achieved through adjusting the Bcd production rate in the anterior (via the adjustment of *bcd* mRNA deposition). Although the models for within-species and between-species Bcd gradient scaling are distinct from each other, they are not mutually exclusive. For example, it is possible (although untested) that the Bcd production rate also differs in embryos from different species.

The proposed adjustment of the Bcd production rate represents a 'passive', self-correcting mechanism in the sense that it may arise as a unidirectional physiological consequence of how nurse cells provision the egg. Although our FISH data clearly demonstrate that large embryos have more *bcd* mRNA than small embryos (Fig. 5 and see Figs S5, S6 and Table S1 in the supplementary material), precisely how this is achieved remains unknown. One could imagine that the rate of *bcd* transcription in nurse cells may be regulated by the cytoplasmic volume through some unknown feedback mechanism(s). Alternatively, the duration of *bcd* transcription (i.e. *bcd* mRNA accumulation) is tightly but passively related to the time that it takes for nurse cells to mature and accumulate their cytoplasmic contents (i.e. cytoplasmic volume) prior to dumping. Our studies described here and previously (He et al., 2008) have focused on embryo size variation that arises from either genetic differences or stochastic fluctuations. However, environmental factors may represent an even more important

determinant of egg size variation. Since the volume-dependent deposition of *bcd* mRNA, and thus the adjustment of Bcd production rate, could take place passively, our proposed Bcd gradient scaling mechanism may also play a role in correcting environmental factor-induced egg size variation. If this is true, this mechanism might represent a general means for scaling (at the level of the Bcd gradient) that is broadly utilized across species.

Bcd gradient scaling achieved by our proposed mechanism is imperfect with respect to certain positions. Although there is good scaling in broad regions of the embryo, there are large differences in *B* in the most anterior parts (Fig. 2B). Such differences lead to large differences in Bcd-encoded positional information (Fig. 2D). How scaled patterning in these parts of the embryo is achieved remains unknown. It is possible that the terminal system may provide positional information in a manner that is also dependent on embryo size. This could be achieved either through a direct, but passive, mechanism, in which the amount of a rate-limiting component(s) of the terminal system is – like *bcd* mRNA – also determined in a volume-dependent manner, or through an indirect feedback mechanism in which the relevant action of this system is regulated by the amount of Bcd (Kim et al., 2010). We also note that, although the *eve* expression boundary positions in the selected large and small embryos have good scaling properties, they do exhibit an allometric shift along the A-P axis (Miles et al., 2010). This shift is not consistent with the shift in the positional information provided by Bcd in this region (the posterior) of the embryo. In addition, when evaluating Bcd gradient properties using the scaling coefficient (de Lachapelle and Bergmann, 2010b), we observed slight hyposcaling in broad regions of the embryo (Fig. 2E and see Fig. S3E in the supplementary material). Together, these results suggest that additional mechanisms, such as the terminal system (Lohr et al., 2009; Ochoa-Espinosa et al., 2009) and/or gene regulatory networks (Bergmann et al., 2007; Jaeger et al., 2004; Manu et al., 2009), work with Bcd to achieve the observed *eve* expression patterns [see also Keranen et al. (Keranen et al., 2006) for pattern flow during embryogenesis].

The deployment of two different mechanisms for achieving Bcd gradient scaling within species versus between species is not surprising in our view. Under sustained evolutionary pressure to maintain Bcd scaling in the face of egg size divergence across species (that require Bcd for A-P patterning), biophysical properties of Bcd gradient formation (i.e. the diffusibility or stability of Bcd) are expected to evolve in concert with embryo size. Over time, and with sufficient fine-tuning of diffusion and degradation rates by natural selection, scaling at all positions can be achieved. By contrast, for the same scaling mechanism to be utilized by embryos of different sizes (of genetic origin) within a species, alleles that control the diffusion or degradation rates of Bcd would have to be tightly associated with the alleles that control embryo size. For a trait such as egg size, with its multifactorial genetic basis, a tight association between egg size and gradient scaling alleles would be difficult, if not impossible, to achieve. Instead, a scaling mechanism achieved through passively adjusting the Bcd production rate provides an effective (though imperfect) means to correct within-species differences in egg size arising from both genetic and stochastic (and possibly environmental) origins.

How a Bcd concentration gradient is formed remains highly controversial (Coppey et al., 2007; Deng et al., 2010; Gregor et al., 2008; Gregor et al., 2007b; Grimm and Wieschaus, 2010; Little et al., 2011; Liu et al., 2011; Liu and Ma, 2011; Porcher et al., 2010; Spirov et al., 2009), even whether the positional information provided by Bcd is decoded before the gradient reaches its steady state (Bergmann et al., 2007; Bergmann et al., 2008; Bialek et al., 2008; de Lachapelle and Bergmann, 2010a; de Lachapelle and Bergmann, 2010b; He et al., 2011; Jaeger, 2010; Liu et al., 2011). Although we have not specifically investigated the process of Bcd gradient formation, the observed scaling properties of the Bcd gradient may be readily explained by a diffusion model if the Bcd production rate is scaled with embryo volume (Deng et al., 2010). It is interesting to note that our observed *S* profile exhibits a broad similarity to the profiles obtained in a model that assumes a volume-dependent Bcd production rate (de Lachapelle and Bergmann, 2010b). Besides the difference in the amount of *bcd* mRNA (and consequently B_0) in the large and small embryos, we currently do not know whether these embryos exhibit other differences that are relevant to Bcd gradient formation. We emphasize that, despite an incomplete knowledge – as a field – of how Bcd gradient formation is controlled, our current study represents a step forward in understanding scaling. Most importantly, the volume-dependent deposition of *bcd* mRNA provides a passive (i.e. self-correcting), early-acting mechanism for producing Bcd scaling that contributes to robust pattern formation. Going beyond the early *Drosophila* embryo, which does not change in overall size as a function of time, morphogen gradients also play roles in patterning tissues that grow in size. A correlation between the amplitude and *L* (achieved by adjusting the morphogen production rate or by other mechanisms) may also provide a simple means to maintain scaled patterning as a tissue grows in size.

Competing interests statement
The authors declare no competing financial interests.

Supplementary material
Supplementary material for this article is available at
http://dev.biologists.org/lookup/suppl/doi:10.1242/dev.064402/-/DC1

References
Bergmann, S., Sandler, O., Sberro, H., Shnider, S., Schejter, E., Shilo, B. Z. and Barkai, N. (2007). Pre-steady-state decoding of the Bicoid morphogen gradient. *PLoS Biol.* **5**, e46.

Bergmann, S., Tamari, Z., Schejter, E., Shilo, B. Z. and Barkai, N. (2008). Re-examining the stability of the Bicoid morphogen gradient. *Cell* **132**, 15-18.

Berleth, T., Burri, M., Thoma, G., Bopp, D., Richstein, S., Frigerio, G., Noll, M. and Nüsslein-Volhard, C. (1988). The role of localization of bicoid RNA in organizing the anterior pattern of the Drosophila embryo. *EMBO J.* **7**, 1749-1756.

Bialek, W., Gregor, T., Tank, D. W. and Wieschaus, E. F. (2008). Response: can we fit all of the data? *Cell* **132**, 17-18.

Burz, D. S., Pivera-Pomar, R., Jackle, H. and Hanes, S. D. (1998). Cooperative DNA-binding by Bicoid provides a mechanism for threshold-dependent gene activation in the Drosophila embryo. *EMBO J.* **17**, 5998-6009.

Coppey, M., Berezhkovskii, A. M., Kim, Y., Boettiger, A. N. and Shvartsman, S. Y. (2007). Modeling the bicoid gradient: diffusion and reversible nuclear trapping of a stable protein. *Dev. Biol.* **312**, 623-630.

de Lachapelle, A. M. and Bergmann, S. (2010a). Pre-steady and stable morphogen gradients: can they coexist? *Mol. Syst. Biol.* **6**, 428.

de Lachapelle, A. M. and Bergmann, S. (2010b). Precision and scaling in morphogen gradient read-out. *Mol. Syst. Biol.* **6**, 351.

Deng, J., Wang, W., Lu, L. J. and Ma, J. (2010). A two-dimensional simulation model of the Bicoid gradient in Drosophila. *PLoS ONE* **5**, e10275.

Driever, W. and Nüsslein-Volhard, C. (1988a). A gradient of bicoid protein in Drosophila embryos. *Cell* **54**, 83-93.

Driever, W. and Nüsslein-Volhard, C. (1988b). The bicoid protein determines position in the Drosophila embryo in a concentration dependent manner. *Cell* **54**, 95-104.

Ephrussi, A. and St. Johnston, D. (2004). Seeing is believing. The bicoid morphogen gradient matures. *Cell* **116**, 143-152.

Flatt, T. (2005). The evolutionary genetics of canalization. *Q. Rev. Biol.* **80**, 287-316.

Gregor, T., Bialek, W., de Ruyter van Steveninck, R. R., Tank, D. W. and Wieschaus, E. F. (2005). Diffusion and scaling during early embryonic pattern formation. *Proc. Natl. Acad. Sci. USA* **102**, 18403-18407.

Gregor, T., Tank, D. W., Wieschaus, E. F. and Bialek, W. (2007a). Probing the limits to positional information. *Cell* **130**, 153-164.

Gregor, T., Wieschaus, E. F., McGregor, A. P., Bialek, W. and Tank, D. W. (2007b). Stability and nuclear dynamics of the bicoid morphogen gradient. *Cell* **130**, 141-152.

Gregor, T., McGregor, A. P. and Wieschaus, E. F. (2008). Shape and function of the Bicoid morphogen gradient in dipteran species with different sized embryos. *Dev. Biol.* **316**, 350-358.

Grimm, O. and Wieschaus, E. (2010). The Bicoid gradient is shaped independently of nuclei. *Development* **137**, 2857-2862.

He, F., Wen, Y., Deng, J., Lin, X., Lu, J., Jiao, R. and Ma, J. (2008). Probing intrinsic properties of a robust morphogen gradient in Drosophila. *Dev. Cell* **15**, 558-567.

He, F., Saunders, T., Wen, Y., Cheung, D., Jiao, R., ten Wolde, P., Howard, M. and Ma, J. (2010a). Shaping a morphogen gradient for positional precision. *Biophys. J.* **99**, 697-707.

He, F., Wen, Y., Cheung, D., Deng, J., Lu, L. J., Jiao, R. and Ma, J. (2010b). Distance measurements via the morphogen gradient of Bicoid in Drosophila embryos. *BMC Dev. Biol.* **10**, 80.

He, F., Ren, J., Wang, W. and Ma, J. (2011). A multiscale investigation of Bicoid-dependent transcriptional events in Drosophila embryos. *PLoS ONE* **6**, e19122.

Hendrikse, J. L., Parsons, T. E. and Hallgrimsson, B. (2007). Evolvability as the proper focus of evolutionary developmental biology. *Evol. Dev.* **9**, 393-401.

Houchmandzadeh, B., Wieschaus, E. and Leibler, S. (2002). Establishment of developmental precision and proportions in the early Drosophila embryo. *Nature* **415**, 798-802.

Jaeger, J. (2010). A matter of timing and precision. *Mol. Syst. Biol.* **6**, 427-428.

Jaeger, J., Surkova, S., Blagov, M., Janssens, H., Kosman, D., Kozlov, K. N., Manu Myasnikova, E., Vanario-Alonso, C. E., Samsonova, M. et al. (2004). Dynamic control of positional information in the early Drosophila embryo. *Nature* **430**, 368-371.

Keranen, S. V., Fowlkes, C. C., Luengo Hendriks, C. L., Sudar, D., Knowles, D. W., Malik, J. and Biggin, M. D. (2006). Three-dimensional morphology and gene expression in the Drosophila blastoderm at cellular resolution II: dynamics. *Genome Biol.* **7**, R124.

Kerszberg, M. and Wolpert, L. (2007). Specifying positional information in the embryo: looking beyond morphogens. *Cell* **130**, 205-209.

Kim, Y., Coppey, M., Grossman, R., Ajuria, L., Jimenez, G., Paroush, Z. and Shvartsman, S. Y. (2010). MAPK substrate competition integrates patterning signals in the Drosophila embryo. *Curr. Biol.* **20**, 446-451.

Kosman, D., Small, S. and Reinitz, J. (1998). Rapid preparation of a panel of polyclonal antibodies to Drosophila segmentation proteins. *Dev. Genes Evol.* **208**, 290-294.

Lander, A. D. (2007). Morpheus unbound: reimagining the morphogen gradient. *Cell* **128**, 245-256.

Little, S. C., Tkacik, G., Kneeland, T. B., Wieschaus, E. F. and Gregor, T. (2011). The formation of the bicoid morphogen gradient requires protein movement from anteriorly localized mRNA. *PLoS Biol.* **9**, e1000596.

Liu, J. and Ma, J. (2011). Fates-shifted is an F-box protein that targets Bicoid for degradation and regulates developmental fate determination in Drosophila embryos. *Nat. Cell Biol.* **13**, 22-29.

Liu, J., He, F. and Ma, J. (2011). Morphogen gradient formation and action: insights from studying Bicoid protein degradation. *Fly (Austin)* **5** (in press).

Lohr, U., Chung, H. R., Beller, M. and Jackle, H. (2009). Antagonistic action of Bicoid and the repressor Capicua determines the spatial limits of Drosophila head gene expression domains. *Proc. Natl. Acad. Sci. USA* **106**, 21695-21700.

Lott, S. E., Kreitman, M., Palsson, A., Alekseeva, E. and Ludwig, M. Z. (2007). Canalization of segmentation and its evolution in Drosophila. *Proc. Natl. Acad. Sci. USA* **104**, 10926-10931.

Ma, X., Yuan, D., Diepold, K., Scarborough, T. and Ma, J. (1996). The Drosophila morphogenetic protein Bicoid binds DNA cooperatively. *Development* **122**, 1195-1206.

Manu, Surkova, S., Spirov, A. V., Gursky, V. V., Janssens, H., Kim, A. R., Radulescu, O., Vanario-Alonso, C. E., Sharp, D. H., Samsonova, M. et al. (2009). Canalization of gene expression in the Drosophila blastoderm by gap gene cross regulation. *PLoS Biol.* **7**, e1000049.

Martinez Arias, A. and Hayward, P. (2006). Filtering transcriptional noise during development: concepts and mechanisms. *Nat. Rev. Genet.* **7**, 34-44.

Miles, C. M., Lott, S. E., Luengo Hendriks, C. L., Ludwig, M. Z., Manu Williams, C. L. and Kreitman, M. (2010). Artificial selection on egg size perturbs early pattern formation in Drosophila melanogaster. *Evolution* **65**, 33-42.

Myasnikova, E., Samsonova, M., Kosman, D. and Reinitz, J. (2005). Removal of background signal from in situ data on the expression of segmentation genes in Drosophila. *Dev. Genes Evol.* **215**, 320-326.

Ochoa-Espinosa, A., Yu, D., Tsirigos, A., Struffi, P. and Small, S. (2009). Anterior-posterior positional information in the absence of a strong Bicoid gradient. *Proc. Natl. Acad. Sci. USA* **106**, 3823-3828.

Otsu, N. (1979). A threshold selection method from gray-level histograms. *IEEE Trans. Syst. Man Cybern.* **9**, 62-66.

Patel, N. H. and Lall, S. (2002). Precision patterning. *Nature* **415**, 748-749.

Patel, N. H., Hayward, D. C., Lall, S., Pirkl, N. R., DiPietro, D. and Ball, E. E. (2001). Grasshopper hunchback expression reveals conserved and novel aspects of axis formation and segmentation. *Development* **128**, 3459-3472.

Porcher, A., Abu-Arish, A., Huart, S., Roelens, B., Fradin, C. and Dostatni, N. (2010). The time to measure positional information: maternal hunchback is required for the synchrony of the Bicoid transcriptional response at the onset of zygotic transcription. *Development* **137**, 2795-2804.

Reinitz, J. (2007). Developmental biology: a ten per cent solution. *Nature* **448**, 420-421.

Spirov, A., Fahmy, K., Schneider, M., Frei, E., Noll, M. and Baumgartner, S. (2009). Formation of the bicoid morphogen gradient: an mRNA gradient dictates the protein gradient. *Development* **136**, 605-614.

Struhl, G., Struhl, K. and Macdonald, P. (1989). The gradient morphogen bicoid is a concentration-dependent transcriptional activator. *Cell* **57**, 1259-1273.

Waddington, C. H. (1942). Canalization of development and the inheritance of aquired characters. *Nature* **150**, 563-565.

Wartlick, O., Kicheva, A. and Gonzalez-Gaitan, M. (2009). Morphogen gradient formation. *Cold Spring Harb. Perspect. Biol.* **1**, a001255.

Weil, T. T., Forrest, K. M. and Gavis, E. R. (2006). Localization of bicoid mRNA in late oocytes is maintained by continual active transport. *Dev. Cell* **11**, 251-262.

Wolpert, L. (1969). Positional information and the spatial pattern of cellular differentiation. *J. Theor. Biol.* **25**, 1-47.

Zhao, C., York, A., Yang, F., Forsthoefel, D. J., Dave, V., Fu, D., Zhang, D., Corado, M. S., Small, S., Seeger, M. A. et al. (2002). The activity of the Drosophila morphogenetic protein Bicoid is inhibited by a domain located outside its homeodomain. *Development* **129**, 1669-1680.